Plasticity-Based Distortion Analysis for Fillet Welded Thin-Plate T-Joints

A new relationship between cumulative plastic strains and angular distortion was found

BY G. H. JUNG AND C. L. TSAI

ABSTRACT. The procedure of plasticity-based distortion analysis (PDA) for directly mapping cumulative plastic strains into elastic models using equivalent thermal strains was developed and applied to the investigation of the characteristic relationship between cumulative plastic strains and angular distortion in fillet welded thin-plate T-joints. Plasticity-based distortion analysis successfully predicted the total angular distortion with an accuracy of 97% compared with angular distortion obtained from the elastic-plastic analysis, demonstrating the validity of the unique relationship between cumulative plastic strains and distortions and the applicability of linear elastic models in welding-induced-distortion analysis. The PDA procedure also provided the quantitative relationship between six cumulative plastic strain components and angular distortion of fillet welded T-joints. Transverse cumulative plastic strain-inducing transverse shrinkage generated bend-down angular distortion, which was different from what has been understood. Vertical and longitudinal cumulative plastic strains produced bend-down and slight bend-up angular distortion, respectively. The major bend-up angular distortion was induced by *xy*-plane shear cumulative plastic strain, which has not been considered as a cause of angular distortion in fillet welded T-joints. Other shear components were not related to angular distortion.

Introduction

From a mechanical viewpoint, distortions and residual stresses induced in structures after welding can be regarded as the resultant of incompatible strains consisting of thermal strains, plastic strains, creep strains, and others. In this study, it is assumed that only plastic strains exist as the incompatible strain after welding, because creep would not be expected due to fast cooling, and no thermal strains are expected after completion of cooling. Therefore, understanding the cumulative plastic strain distribution after welding can be regarded as a linchpin of residual stress and distortion analysis.

Ueda and his coworkers (Refs. 1–4) defined the characteristic distribution of inherent strains, and applied it to predict residual stresses induced by welding. Based on experimental, theoretical, and numerical studies, they defined inherent strain distributions using a trapezoid curve pattern, and predicted residual stresses by performing the elastic analysis, in which equivalent distributed loads replaced inherent strains. Others (Refs. 5–7) applied this method to predict welding-induced distortion. This inherent strain approach was based on the assumption that residual stresses and distortions being analyzed should be uniquely predicted by the specifically selected component of inherent strains. For example, if longitudinal inherent strain were used in the prediction of longitudinal residual stress or distortion, other inherent strain components should not affect longitudinal residual stress or distortion, or their effect should be small enough to be negligible. Therefore, it is critical to understand the relationship between cumulative plastic strains and distortions/residual stresses in the application of the inherent strain approach.

In terms of angular distortion, it has been believed that angular distortion is induced by transverse cumulative plastic strain, which is distributed nonuniformly through the thickness of a plate. This statement may be true in the case of welded butt joints, but Han (Ref. 8) found that angular distortion in butt joints resulted not only from transverse cumulative plastic strain, but also from a longitudinal component, according to his observation of the evolution of angular distortion and cumulative plastic strains. On the other hand, for fillet welded T-joints, which have more complex geometric configurations than welded butt joints, only a few studies (Refs. 3, 9, 10) have been performed to figure out the angular distortion mechanism using numerical and experimental analyses. They explained the angular distortion mechanism using the change of the location of the shrinkage source. It seems those researchers believed the gradient of transverse shrinkage resulted in angular distortion in fillet welded joints like welded butt joints. For the application of the inherent strain approach to T-joints, Yuan and Ueda (Ref. 4) used it to predict longitudinal residual stress in T-joints and I-beam cross-section joints, but no further research on the prediction of angular distortion of T-joints has been done. Some difficulties or misunderstandings may restrict the application of the inherent strain approach to the prediction of angular distortion in fillet welded T-joints.

As mentioned above, it is critical to postulate the characteristic relationship between cumulative plastic strains and angular distortion in order to provide better quantitative understanding of the angular distortion mechanism. In this study, a new approach analyzing the relationship between cumulative plastic strains and angular distortion in fillet welded T-joints, dubbed "plasticity-based distortion analysis," is proposed and applied to the investigation of the relationship between cumulative plastic strains and angular distortion in fillet welded thin-plate T-joints.

KEYWORDS

Plasticity-Based Distortion
Numerical Analysis
Finite Element Model
Fillet Welds
Weld Process Simulation

G. H. JUNG is with the Edison Welding Institute, Columbus, Ohio. C. L. TSAI is with Industrial, Welding and Systems Engineering at The Ohio State University, Columbus, Ohio.

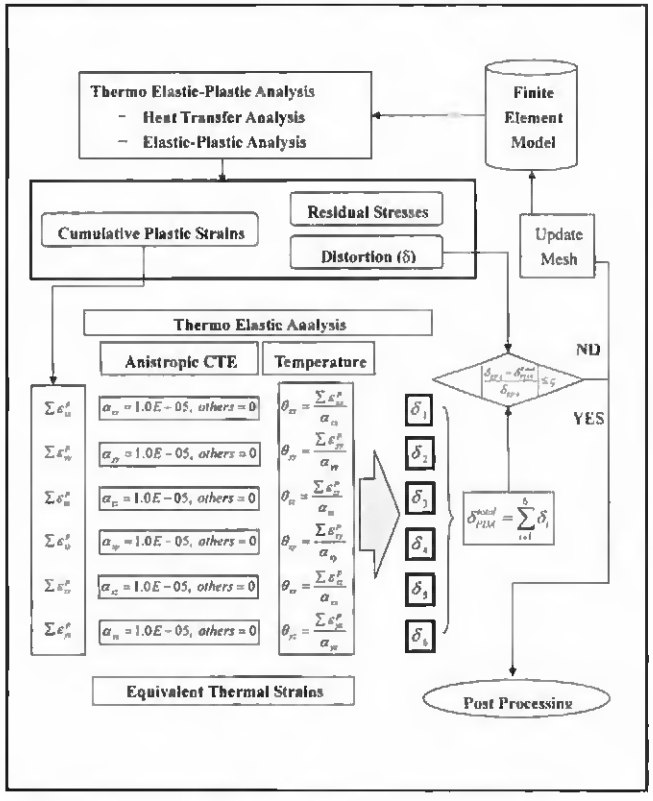

Fig. 1 — Procedure of plasticity-based distortion analysis (PDA).

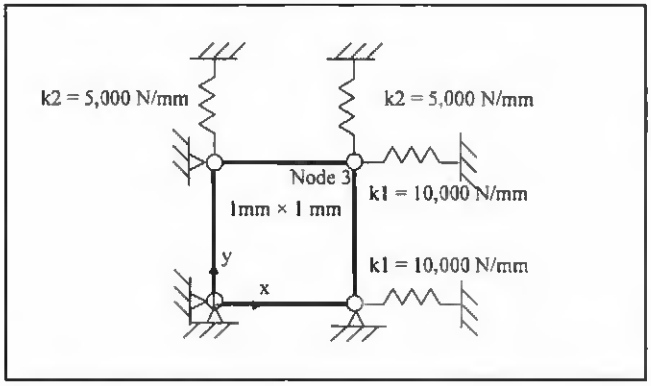

Fig. 2 — Simple 2-D FE model.

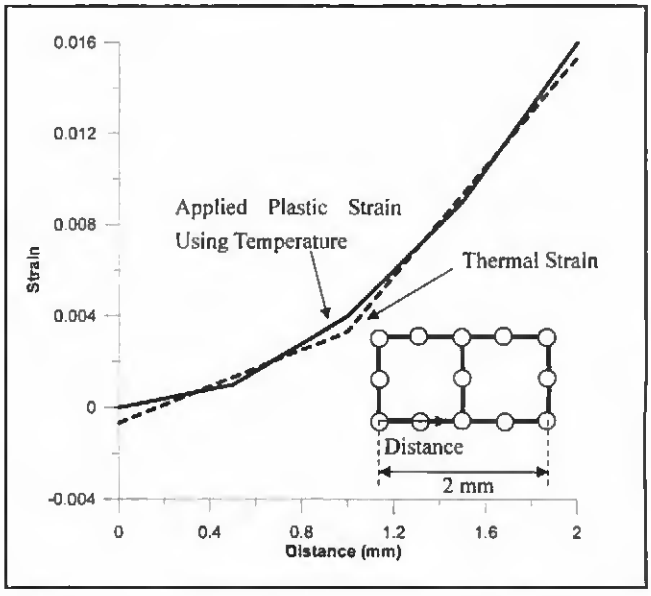

Fig. 3 — Characteristics of thermal strain in second-order elements.

The Procedure of Plasticity-Based Distortion Analysis

Plasticity-hased distortion analysis (PDA) is a numerical procedure to predict welding-induced distortion by direct mapping characteristic cumulative plastic strains into elastic models, instead of applying equivalent forces and moments. One of the advantages of this approach is to incorporate all cumulative plastic strain components in predicting distortion, and investigate the relationship between each cumulative plastic strain and a distortion type of concern. Especially for fillet welded T-joints, which are complex in geometric configuration, PDA becomes a more powerful tool.

General Procedure of PDA

Figure 1 shows the flow chart of PDA consisted of three parts:

Part 1: Thermal-elastic-plastic analysis (EPA), determining the characteristic cumulative plastic strain distribuhons of all six components and distortions.

Part 2: Elastic analysis, calculating individual distortions corresponding to the mapped individual cumulative plastic strains. Repeat six times with all components of cumulative plastic strains in the case of a 3-D model, and four times for a generalized plane strain model.

Part 3: Post-processing, obtaining the total distortion by adding individual distortions induced by each cumulative plastic strain component.

In Part 1, PDA requires the appropriate distributions of all cumulative plastic components from the thermal-elastic-plastic analysis for the given welding condition. It was assumed that the present thermal-elastic-plastic analysis with an initial finite element model would predict the reasonable distortion pattern, and the change of the number of nodes and elements would not significantly affect the characteristic distribution pattern of cumulative plastic strains.

Part 2 is an elastic analysis. Each cumulative plastic strain distribution obtained from the thermal-elastic-plastic analysis was mapped into elastic models using the equivalent incompatible strain fields, such as thermal strains. Thermal strains can be dependent on temperature or field variahles. In this study, temperature and the corresponding thermal expansion coefficient were used to generate thermal strains. For the 3-D model, six components of cumulative plastic strains were mapped one by one into six elastic models using corresponding temperature fields, and six individual distortions were determined from the six elastic analyses.

In Part 3, the relationship between cumulative plastic strains and distortion can be explained with quantitative measure, and the accuracy of the PDA procedure can he checked. Each individual distortion represents the contribution of each cumulative plastic strain to total distortion. The total distortion can be calculated by adding six individual distortions, comparing the total distortion with the distortion obtained from the thermal-elastic-plastic analysis in order to check the accuracy of the PDA procedure. If the accuracy does not satisfy the required accuracy in terms of the engineering application, Parts 1, 2, and 3 should be repeated with the remeshed finite element model until the accuracy is acceptable. At this point, it is assumed that the accuracy is mainly dependent upon the mesh pattern.

Mapping Method

After completing heating and cooling, six components of cumulative plastic strains exist as incompatible strains and result in distortion. The equivalent thermal strains induced by thermal expansion, plastic strains, or other field variables causing straining of materials may be considered as incompatible strains. In this study, the equivalent thermal strains were used as incompatible strains replacing the effect of cumulative plastic strains.

Using anistropic thermal expansion coefficients and corresponding temperature fields, each cumulative plastic strain component can be mapped independently into six elastic models. For example, transverse cumulative plastic strain, $\Sigma\varepsilon^p_{xx}(x,y,z)$, can be mapped by using the temperature field calculated by Equation 1.

$$\theta_{xx}(x,y,z)=\frac{\sum\varepsilon^p_{xx}(x,y,z)}{\alpha_{xx}}$$
$$\alpha_{xx}=\text{constant},\alpha_{yy}=\alpha_{zz}=\alpha_{xy}=\alpha_{xz}=\alpha_{yz}=0 \quad (1)$$

where θ is temperature and α is anistropic thermal expansion coefficients. Other temperature fields associated with other cumulative plastic strain components can be obtained in the same way using Equation 1.

In order to obtain corresponding temperature fields, a FORTRAN program was developed to retrieve all cumulative plastic strains (averaged at nodes) over all nodes from the thermal-elastic-plastic analysis, and the program saved them into a data file. Using the data file containing cumulative plastic strain values at all nodes, corresponding temperature values at all nodes were calculated using a user-subroutine "UTEMP" and Equation 1 (Refs. 11, 12).

Six cumulative plastic strains can also be simultaneously mapped into an elastic model using the equivalent thermal strains depending upon six field variables. These equivalent thermal strains can be calculated by user-subroutines "UFIELD" and "UEXPAN" using Equation 2 (Ref.11).

$$\varepsilon^{th}_{ij}=\alpha_{ij}F_{ij}(x,y,z)$$
where,
$$F_{ij}(x,y,z)=\frac{\sum\varepsilon^p_{ij}(x,y,z)}{\alpha_{ij}}:\text{FieldVariables} \quad (2)$$

This simultaneous mapping method was used to demonstrate the validity of the addition procedure to obtain the total distortion and the unique relationship between cumulative plastic strains and distortions.

Table 1 — Comparison of Results from EPA and PDA

Type of Analysis	Mapped Component	Stress (MPa) S_{xx}	S_{yy}	S_{zz}	Mises	Displacement (mm) U_x	U_y
EPA		5.86	–5.36	17.73	20.00	–2.928E-04	5.359E-04
PDA	$\Sigma\varepsilon^p_{xx}$	4.61	0.46	1.52	3.73	–2.305E–04	–4.598E–05
PDA	$\Sigma\varepsilon^p_{yy}$	–1.20	–7.41	–2.58	5.65	5.997E–05	7.412E–04
PDA	$\Sigma\varepsilon^p_{zz}$	2.45	1.59	18.79	16.00	–1.223E–04	–1.593E–04
PDA	Sum	5.86	–5.36	17.73		–2.928E–04	5.359E–04

Table 2 — Comparison of Results from PDA and Simultaneous Mapping Analysis

Case	Mapped Component	Stress (MPa) S_{xx}	S_{yy}	S_{zz}	Mises	Displacement (mm) U_x	U_y
1	$\Sigma\varepsilon^p_{xx}$	4.61	0.46	1.52	3.73	–2.305E–04	–4.598E–05
	$\Sigma\varepsilon^p_{yy}$	–1.20	–7.41	–2.58	5.65	5.997E–05	7.412E–04
	Sum	3.41	–6.95	–1.06		–1.705E–04	6.952E–04
	$\Sigma\varepsilon^p_{xx}+\Sigma\varepsilon^p_{yy}$	3.41	–6.95	–1.06		–1.705E–04	6.952E–04
2	$\Sigma\varepsilon^p_{xx}$	4.61	0.46	1.52	3.73	–2.305E–04	–4.598E–05
	$\Sigma\varepsilon^p_{zz}$	2.45	1.59	18.79	16.00	–1.223E–04	–1.593E–04
	Sum	7.06	2.05	20.31		–3.528E–04	–2.053E–04
	$\Sigma\varepsilon^p_{xx}+\Sigma\varepsilon^p_{zz}$	7.06	2.05	20.31		–3.528E–04	–2.053E–04
3	$\Sigma\varepsilon^p_{yy}$	4.61	0.46	1.52	3.73	–2.305E–04	–4.598E–05
	$\Sigma\varepsilon^p_{zz}$	–1.20	–7.41	–2.58	5.65	5.997E–05	7.412E–04
	Sum	3.41	–6.95	–1.06		–1.705E–04	6.952E–04
	$\Sigma\varepsilon^p_{yy}+\Sigma\varepsilon^p_{zz}$	3.41	–6.95	–1.06		–1.705E–04	6.952E–04
4	$\Sigma\varepsilon^p_{xx}$	4.61	0.46	1.52	3.73	–2.305E–04	–4.598E–05
	$\Sigma\varepsilon^p_{yy}$	–1.20	–7.41	–2.58	5.65	5.997E–05	7.412E–04
	$\Sigma\varepsilon^p_{zz}$	–1.20	–7.41	–2.58	5.65	5.997E–05	7.412E–04
	Sum	5.86	–5.36	17.73		–2.928E–04	5.359E–04
	$\Sigma\varepsilon^p_{xx}+\Sigma\varepsilon^p_{yy}+\Sigma\varepsilon^p_{zz}$	5.86	–5.36	17.73		–2.928E–04	5.359E–04

PDA: Sum. Simultaneous mapping analysis: $\Sigma\varepsilon^p_{xx}+\Sigma\varepsilon^p_{yy}$, $\Sigma\varepsilon^p_{xx}+\Sigma\varepsilon^p_{zz}$, $\Sigma\varepsilon^p_{yy}+\Sigma\varepsilon^p_{zz}$, $\Sigma\varepsilon^p_{xx}+\Sigma\varepsilon^p_{yy}+\Sigma\varepsilon^p_{zz}$.

Accuracy of PDA Procedure

As a final step of PDA, the total distortion induced by all cumulative plastic strains is obtained by adding individual distortions calculated from six independent elastic analyses:

$$\delta^{total}_{PDA}=\sum_{i=1}^{6}\delta_i \quad (3)$$

where δ^{total}_{PDA} is the total distortion, and δ_i is individual distortion with only i^{th} component of cumulative plastic strains. The accuracy of the PDA procedure can be determined by comparing distortions from the elastic-plastic analysis with the total distortion obtained from the PDA using Equation 3.

$$\text{Error}=\left|\frac{\delta_{EPA}-\delta^{total}_{PDA}}{\delta_{EPA}}\right|\times 100(\%) \quad (4)$$

Table 3 — Material Constants for Kinematic Nonlinear Hardening

Temperature (Δ°C)	Yield Strength (MPa)	C_0 (MPa)	γ
21	145	3714	27
70	145	2800	27
225	84	1300	27
325	45	600	27
400	15	10	27
470	5	1	27
595	5	1	27

This accuracy of the PDA procedure may be affected by some factors, such as nonlinearity of material and mapping accuracy.

One factor is nonlinearity of material, which does not allow linear supposition if the effect of nonlinearity is dominant. Material nonlinearity comes from plastic de-

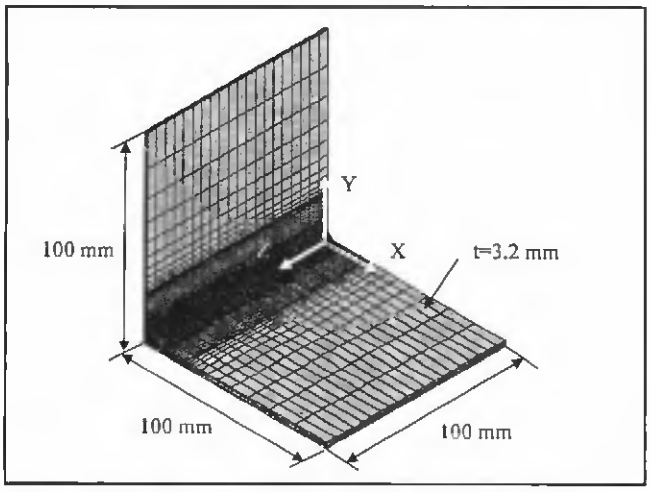

Fig. 4 — Symmetric-half finite element model for the T-joint.

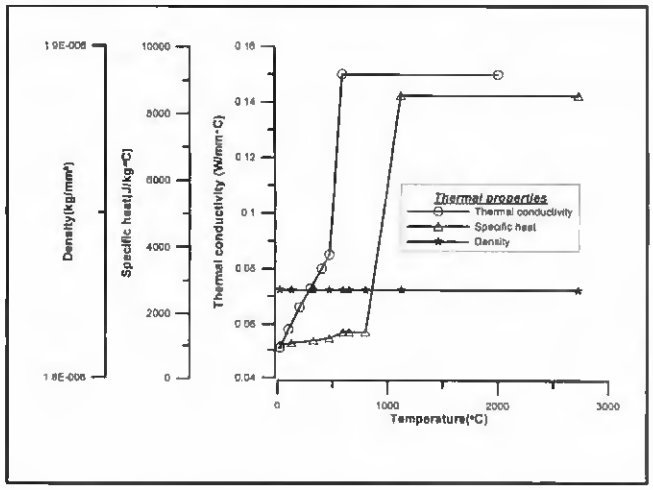

Fig. 5 — Temperature-dependent thermal material properties of magnesium alloy, AZ 91 C.

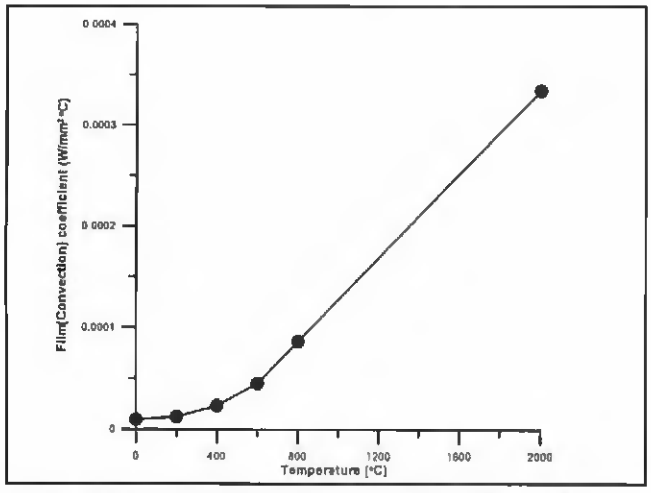

Fig. 6 — Temperature-dependent natural convection (film) coefficients.

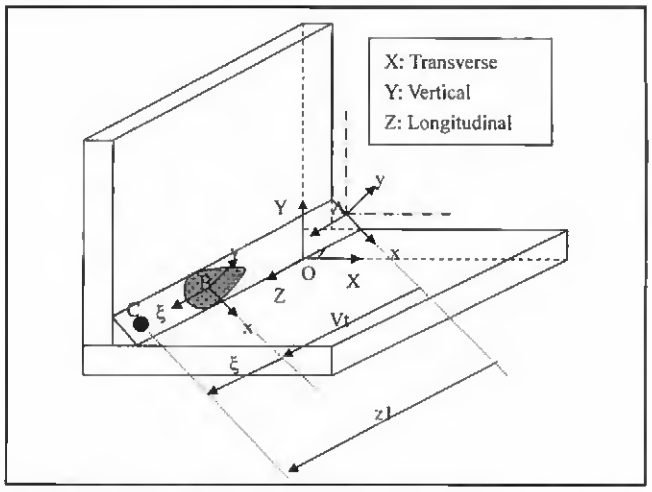

Fig. 7 — Definition of a moving coordinate system (x,y,ξ) in the T-joint.

formation and temperature dependency in a welding situation. In the PDA, material nonlinearity due to temperature dependency does not exist anymore, because temperature is constant (room temperature) after completing welding. Nonlinearity due to plastic deformation can also be negligible because the PDA is somewhat elastic, reloading analysis up to the final plastic deformation after welding.

In order to demonstrate the effect of material nonlinearity on the PDA accuracy, a 2-D simple plain strain model is used as shown in Fig. 2. For this analysis, cumulative plastic strains are perfectly mapped because they are uniformly distributed. Elastic modulus, yield stress, Poisson's ratio, and thermal expansion coefficient are 30E3 MPa, 20 MPa, 0.3, and 1.0E-5, respectively. They are constant during heating and cooling. No strain hardening occurs during plastic deformation. The uniform temperature is applied on an element, increasing linearly to 1000°C from 0°C, and decreasing to 0°C. Three-axial stress state is generated by using different spring constants, $k1$ = 1.0E5 (N/mm) and $k2$ = 0.50E5 (N/mm). The obtained cumulative plastic strains are –0.3643E–03, 0.9504E–03, –0.5861E–03, and 0.0 in the x, y, z, and xy directions, respectively. All components of stresses and displacements in an element at Node 3 are listed in Table 1. Each cumulative plastic strain was mapped into an elastic model one by one. Stresses and displacements obtained from the PDA are listed and compared in Table 1. In the case with the uniform cumulative plastic strain distribution, the PDA calculates the exact stresses and displacements. Therefore, material nonlinearity may not affect the accuracy of the PDA.

In order to demonstrate the unique relationship between cumulative plastics and distortion, the simultaneous mapping analysis was performed under the combined cumulative plastic strains. Table 2 shows that the final stresses and displacements obtained from the simultaneous mapping analysis are equal to those calculated by the PDA, which satisfies the linear superposition requirement described in Equation 5. Therefore, it can be said that each individual displacement (distortion) and stress can be uniquely determined by the associated cumulative plastic strain.

$$L\begin{pmatrix}\sum\varepsilon^{p}_{xx},\sum\varepsilon^{p}_{yy},\sum\varepsilon^{p}_{zz},\\ \sum\varepsilon^{p}_{xy},\sum\varepsilon^{p}_{xz},\sum\varepsilon^{p}_{yz}\end{pmatrix} = L_1\left(\sum\varepsilon^{p}_{xx}\right)+L_2\left(\sum\varepsilon^{p}_{yy}\right)+L_3\left(\sum\varepsilon^{p}_{zz}\right) +L4\left(\sum\varepsilon^{p}_{xy}\right)+L_5\left(\sum\varepsilon^{p}_{xz}\right)+L_6\left(\sum\varepsilon^{p}_{yz}\right) \quad (5)$$

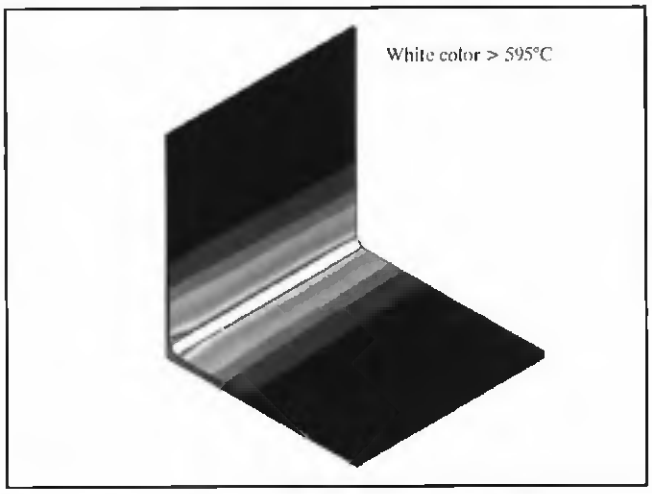

Fig. 8 — Maximum peak temperature map in the T-joint.

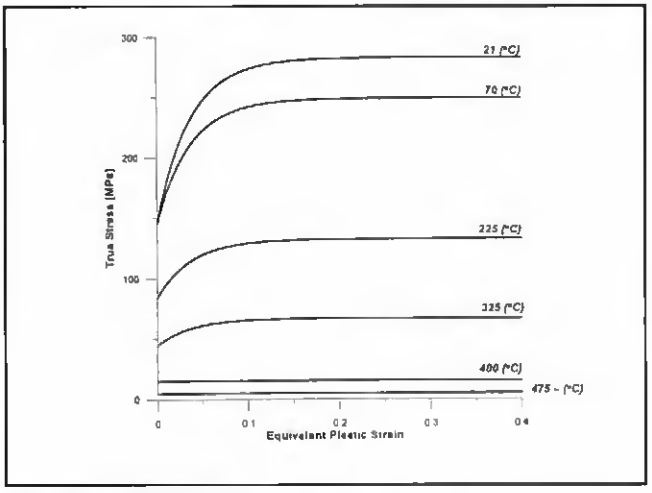

Fig. 9 — Temperature-dependent nonlinear kinematic strain-hardening model of magnesium alloy.

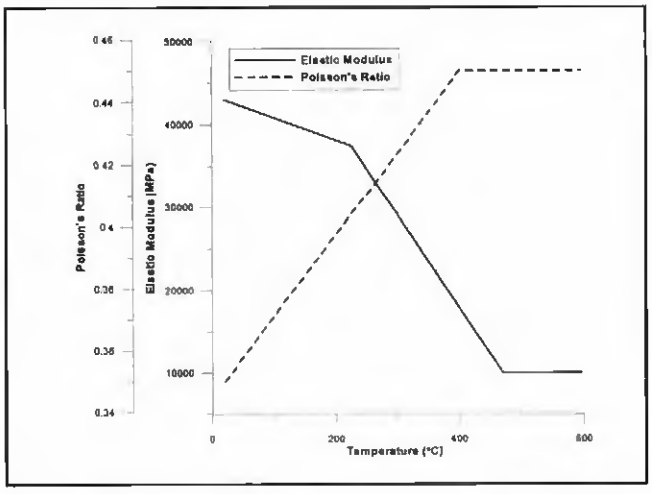

Fig. 10 — Temperature-dependent elastic modulus and Poisson's ratio of magnesium alloy.

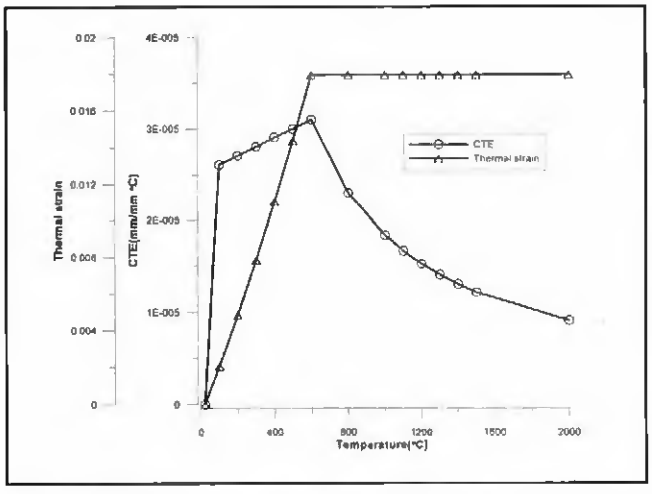

Fig. 11 — Temperature-dependent CTE and corresponding thermal strain of magnesium alloy.

Geometric nonlinearity does not exist in this study because the small deformation theory is used in both the EPA and the PDA.

Mapping accuracy may also affect the accuracy of the PDA procedure. If cumulative plastic strains were not precisely mapped, individual and total angular distortions calculated from the PDA would not be correct. Mapping accuracy is strongly dependent upon the number of elements/nodes and the order of shape function of element. Figure 3 shows the applied cumulative plastic strain using temperature and the calculated thermal strain within two second-order elements in which thermal strain is linear. It shows that unless cumulative plastic strains are distributed uniformly or linearly within an element, mapping error is unavoidable, even though second-order elements are used. The averaged cumulative plastic strains at nodes may also result in error when the significant discontinuity of cumulative plastic strains at integration points between adjacent elements is present. In order to reduce the error induced by mapping, a finer meshed model with second-order elements is recommended.

In this study, it is assumed that the acceptable error range of the PDA procedure was 0% to 10% in view of the engineering application. Since most error comes from the mapping, the finite element model used in the EPA and the PDA should be updated until the required accuracy is achieved.

Numerical 3-D Thermal-Elastic-Plastic Analysis

In thermal-elastic-plastic analysis, the effects of more complex behaviors in welding, such as metallurgical transformation, stress and strain relaxation at the melting temperature, filler metal deposition, etc., were not considered in this analysis. Without considering these effects, the present thermal-elastic-plastic analysis predicted the reasonable angular distortion of an aluminum T-joint compared with the published experimental results (Ref. 12). Therefore, it can be assumed that the present analysis procedure provides the reasonable baseline information, such as the characteristic distribution patterns of cumulative plastic strains and the corresponding angular distortion in fillet welded T-joints.

Two fillet welds running simultaneously at two sides constructed a T-joint. Welding parameters of gas metal arc welding were voltage of 13 V, current of 110 A, and weld speed of 10 mm/s for 3.2-mm-thick magnesium alloy (AZ91 C) plates (Ref. 13). ABAQUS 5.8-14 was used in the following thermal-elastic-plastic analysis.

Thermal Analysis

Quadratic brick elements with 20 nodes were used. The total numbers of el-

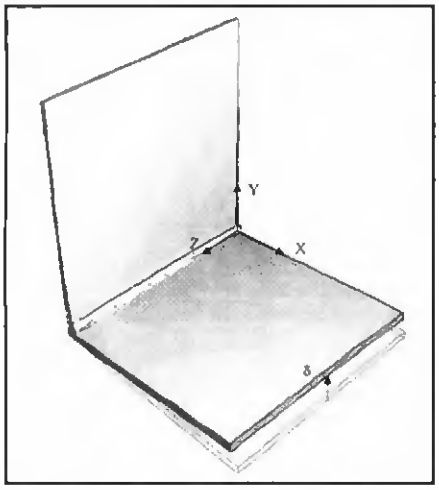

Fig. 12 — Deformed shape of the T-joint after welding.

Table 4 — Comparison of the Averaged Displacements Obtained from EPA, PDA, and Simultaneous Mapping Analysis for a T-Joint

Type of Analysis		Displacement (mm) U_X	U_Y	U_Z
EPA		–2.090E–01	1.042E+00	1.328E–01
PDA	$\Sigma\varepsilon^P_{xx}$	–1.694E–01	–1.143E+00	1.028E–01
	$\Sigma\varepsilon^P_{yy}$	1.202E–02	–7.656E–01	5.590E–04
	$\Sigma\varepsilon^P_{zz}$	–2.263E–04	8.392E–02	5.364E–03
	$\Sigma\varepsilon^P_{xy}$	–4.991E–02	2.805E+00	1.088E–03
	$\Sigma\varepsilon^P_{xz}$	–3.316E–04	9.435E–03	1.627E–01
	$\Sigma\varepsilon^P_{yz}$	–4.742E–04	1.995E–02	–1.399E–01
	SUM	–2.084E–01	1.009E+00	1.327E–01
Simultaneous Mapping		–2.084E–01	1.009E+00	1.327E–01

ements and nodes used were 6100 and 30068, respectively. Figure 4 shows a symmetric-half finite element model used in the thermal analysis for the fillet welded T-joint, with a flange of 100 × 200 × 3.2 mm, and a web erected on the flange plate of 100 × 100 × 3.2 mm.

Figure 5 shows the temperature-dependent thermal-material properties of AZ91 C (Ref. 14). Latent heat, solidus temperature, and liquidus temperature are 3.73E5 J/(kg·°C), 470°C, and 595°C, respectively. Natural convection boundaries shown in Fig. 6 were described on the entire free surfaces of the joint except for a symmetric plane.

A user-subroutine in ABAQUS, "DFLUX" (Ref. 11), was written to incorporate the effect of the moving heat defined by the double ellipsoidal distribution (Ref. 15), the moving coordinate, and the coordinate transformation using Equations 6 and 7.

$$\xi \geq 0,\ q(x,y,\xi) = \frac{6\sqrt{3}r_f \eta VI}{abc_f\pi\sqrt{\pi}} \exp\left(-\frac{3x^2}{a^2}-\frac{3y^2}{b^2}-\frac{3\xi^2}{c_f^2}\right) \quad \text{[Front region]} \qquad (6)$$

$$\xi < 0,\ q(x,y,\xi) = \frac{6\sqrt{3}r_b \eta VI}{abc_b\pi\sqrt{\pi}} \exp\left(-\frac{3x^2}{a^2}-\frac{3y^2}{b^2}-\frac{3\xi^2}{c_b^2}\right) \quad \text{[Rear region]} \qquad (7)$$

where η is arc efficiency, V is voltage, I is current, (x,y,ξ) are moving coordinates (see Fig. 7). Parameters in Equations 6 and 7 for fillet welded T-joints with 3.2 mm of weld leg in fillet welds (Ref. 16) are

$$a = b = 3.2 \cdot \sin(45)$$
$$c_f = a,\quad c_b = 2a$$
$$r_f = \frac{2c_f}{c_f + c_b},\quad r_b = \frac{2c_b}{c_f + c_b}$$

In order to predict distortion patterns induced by welding, it is critical to obtain the reasonable temperature evolution without the significant loss of accuracy. For fillet welded joints, heat input calibration was carried out by matching the boundary of the molten pool with the predesigned fillet size. In order to obtain the boundary of the molten pool, a user-subroutine, "UVARM" (Ref. 11), was developed to calculate the maximum peak temperature over all nodes. Figure 8 shows a map of the maximum peak temperature after welding calculated by UVARM. For the given welding conditions and finite element meshes, arc efficiency (η) was 0.6, which includes the effects of the arc efficiency itself, as well as the heat loss during scanning heat distribution onto the discrete finite elements.

Elastic-Plastic Mechanical Analysis

The main purpose of the elastic-plastic mechanical analysis is to obtain the characteristic cumulative plastic strain distribution patterns and the associated angular distortion for fillet welded thin-plate T-joints. In the elastic-plastic mechanical analysis, the same finite element model used in the thermal analysis was used. The temperature evolution was retrieved from the thermal analysis.

In the thermal-elastic-plastic analysis, it has been known that the most difficult part is to obtain the appropriate material properties at the elevated temperature. Especially for special and rare alloys, it is very hard to find the material database applicable at the elevated temperature. For the magnesium alloy AZ91 C, only a few material properties at the elevated temperature are available from metals handbooks. Dependency of elastic modulus, yield strength, and tensile strength on temperature may give a significant impact on cumulative plastic strains and distortion patterns.

In this study, temperature dependency of mechanical material properties of AZ91 C were taken from that of other applicable magnesium alloys at elevated temperatures (Ref. 17). Figures 9, 10, and 11 show mechanical properties depending on temperature. It was assumed that thermal strain over melting temperature was constant. Thermal expansion coefficients associated with this were modified as shown in Fig. 11. Nonlinear kinematic strain hardening proposed by Chaboche (Refs. 11, 18) was used to consider the effect of a cyclic loading (heating and cooling), as shown in Fig. 9. Back-stress evolution is used to define the kinematic strain hardening model, which is

$$\alpha = \frac{C_0}{\gamma}\left(1 - e^{-\gamma\bar{\varepsilon}^{pl}}\right) \qquad (8)$$

where C_0 is a material constant representing initial kinematic hardening modulus; γ is a material constant determining the rate at which the kinematic hardening modulus decreases with increasing plastic deformation; and $\bar{\varepsilon}^{pl}$ is equivalent plastic strain. These material constants are listed in Table 3.

The top edge of the web plate, $Y = 100$ mm in Fig. 4, was fixed during welding and cooling. Symmetric boundary conditions were applied in the YZ plane at $X = 0$ mm.

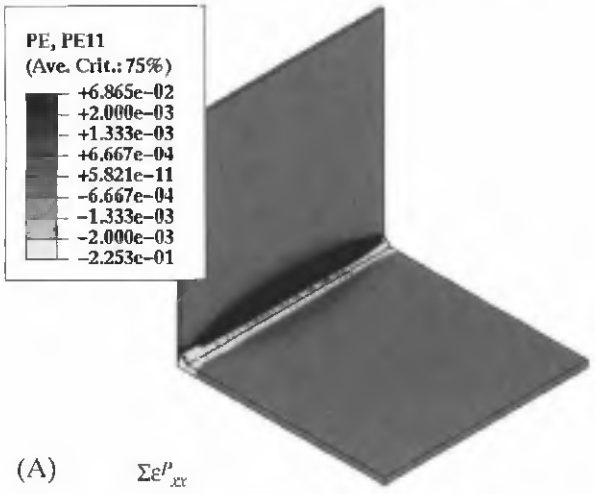

(A) $\Sigma\varepsilon^{P}_{xx}$

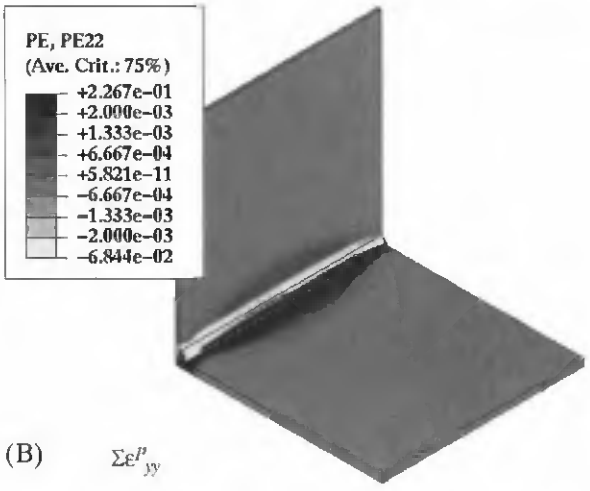

(B) $\Sigma\varepsilon^{P}_{yy}$

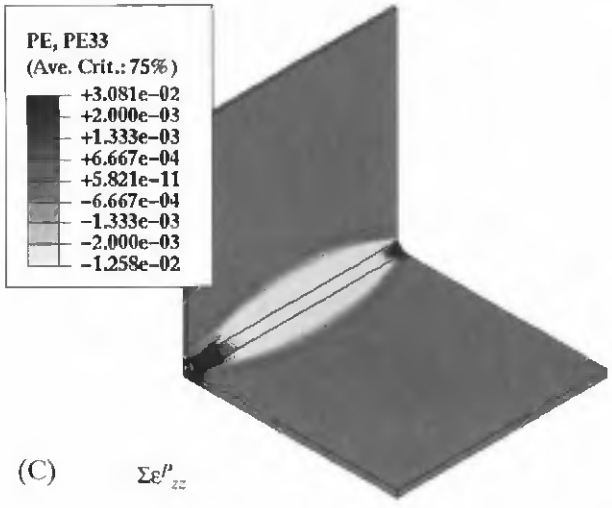

(C) $\Sigma\varepsilon^{P}_{zz}$

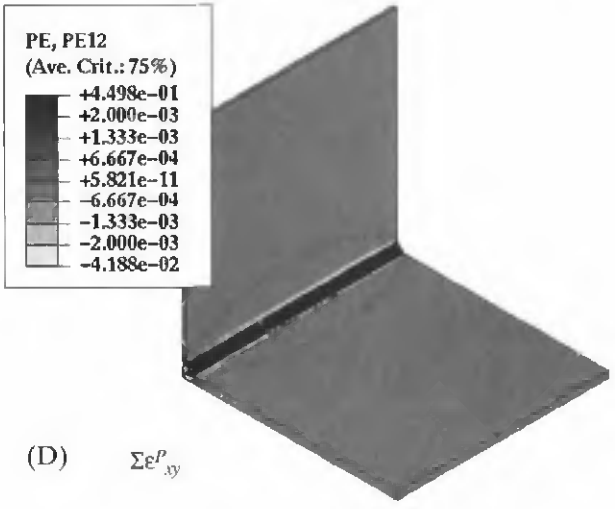

(D) $\Sigma\varepsilon^{P}_{xy}$

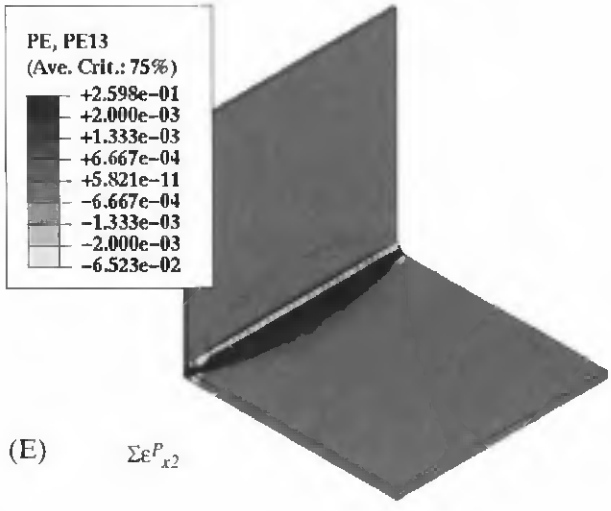

(E) $\Sigma\varepsilon^{P}_{x2}$

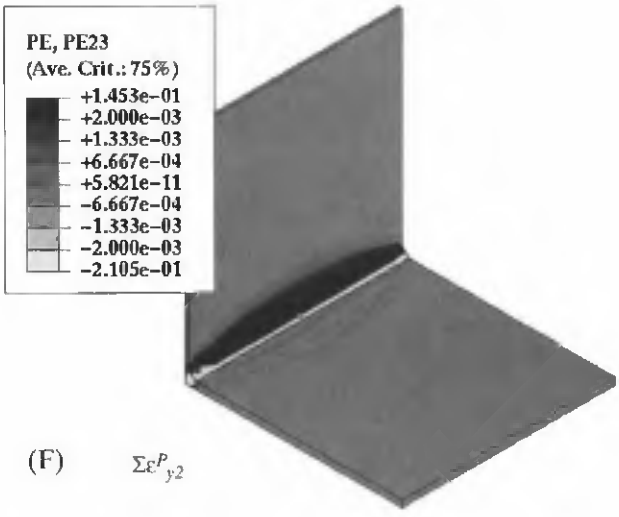

(F) $\Sigma\varepsilon^{P}_{y2}$

Fig. 13 — Cumulative plastic strain maps in the T-joint.

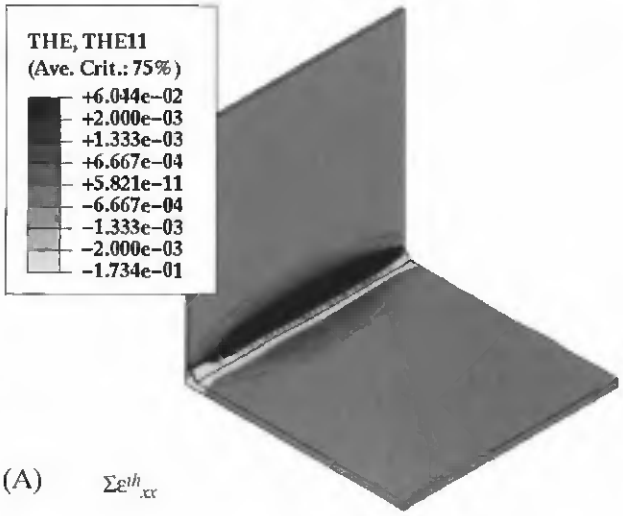

(A) $\Sigma\varepsilon^{th}_{xx}$

(B) $\Sigma\varepsilon^{th}_{yy}$

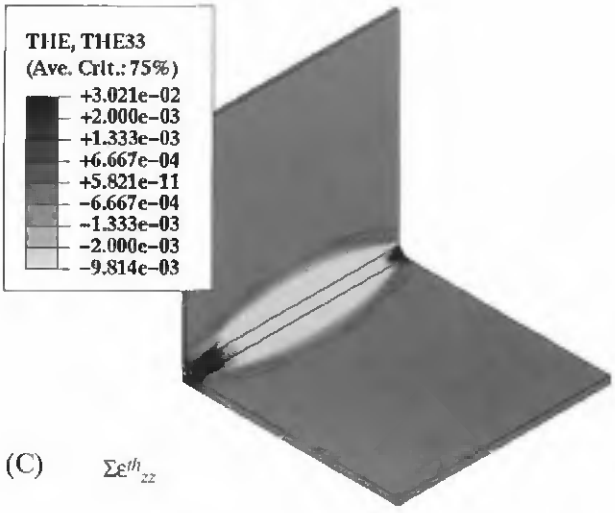

(C) $\Sigma\varepsilon^{th}_{zz}$

(D) $\Sigma\varepsilon^{th}_{xy}$

(E) $\Sigma\varepsilon^{th}_{xz}$

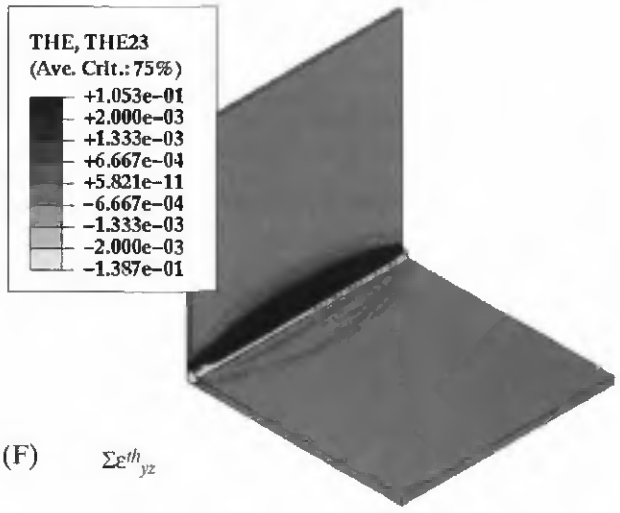

(F) $\Sigma\varepsilon^{th}_{yz}$

Fig. 14 — Equivalent thermal strain maps in the T-joint.

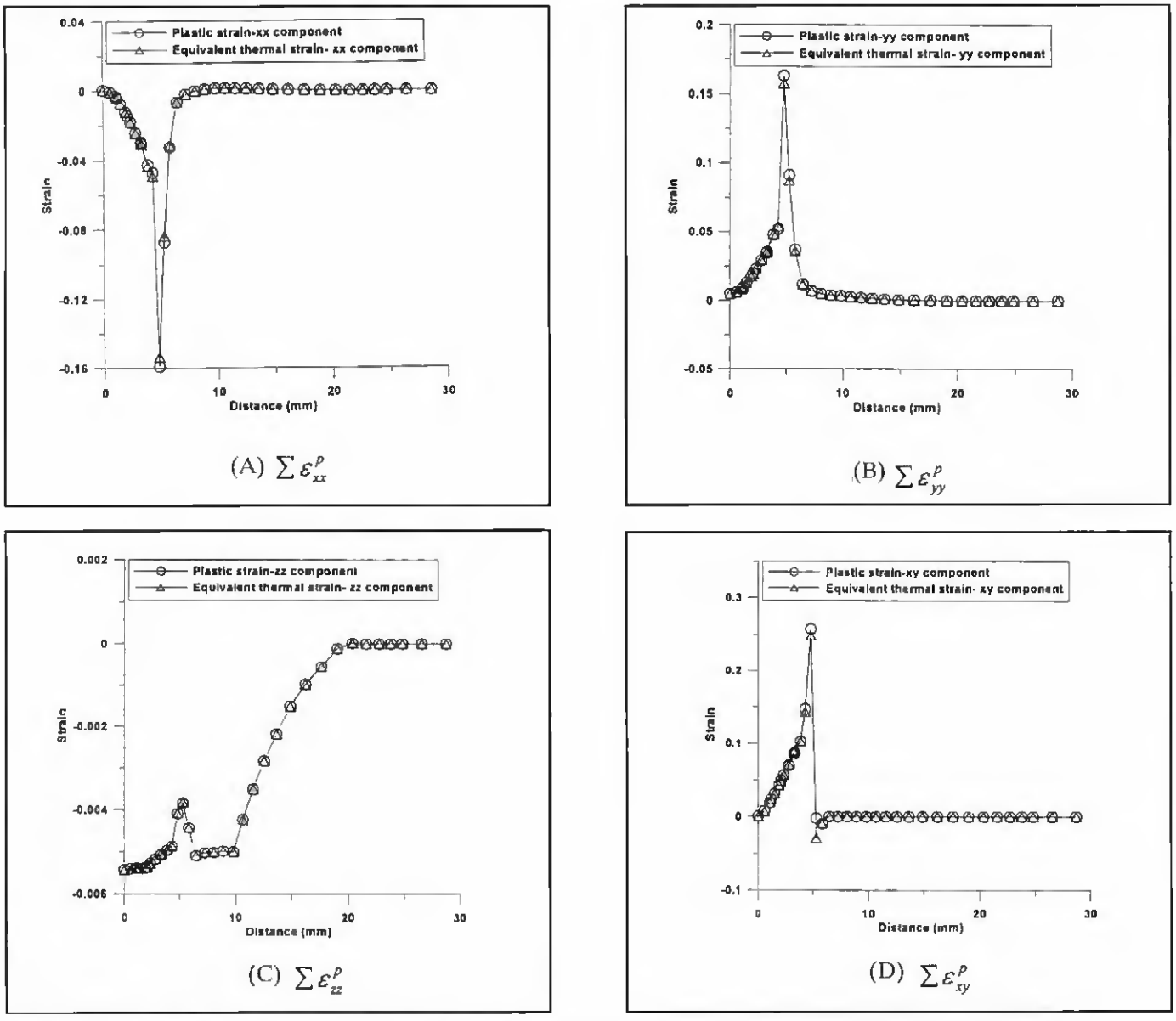

Fig. 15 — Comparison of cumulative plastic strains and equivalent thermal strains.

Results of Thermal-Elastic-Plastic Analysis

Figure 2 shows the deformed shape after welding and cooling. Significant bend-up angular distortion is observed. Angular distortion can be interpreted by displacement in the *Y*-direction. The maximum angular distortion along the free edge of the flange plate is $\delta = 1.05$ mm at its mid-span of $Z = 50$ mm. It is shown that angular distortion at the weld stop is smaller than at the weld start.

Six components of cumulative plastic strains are plotted in Fig. 13 with the same color contour spectrum. The range of the color spectrum is the same for all contour plots: maximum band = +0.002 ~ max.; minimum band = min. ~ –0.002. It has been reported that the transverse cumulative plastic strain shown in Fig. 13A is mainly related to angular distortion when it has the gradient through the plate thickness (Refs. 10, 19). The longitudinal component has been realized as a main source related to longitudinal bending and buckling. To date, three shear components shown in Fig. 13 D–F have not been highlighted in any distortion analysis.

Results of Plasticity-Based Distortion Analysis (PDA)

Cumulative plastic strains obtained from the thermal-elastic-plastic analysis were mapped into elastic models with elastic modulus, 4.3E04 (MPa), and Poisson's ratio, 0.35, at room temperature using the equivalent thermal strains. Figure 14 shows the equivalent thermal strain contours mapped into elastic models. Four components of cumulative plastic strains and equivalent thermal strains on the top surface of the flange plate at $Z = 50$ mm are plotted and compared in detail, as shown in Fig. 15. Even though there are some differences in magnitude of cumulative plastic strains and equivalent thermal strains near the weld region, the general distribution patterns are very close to each other.

Six deformed shapes related to each cumulative plastic strain were obtained and plotted in Fig. 16. What was expected and previously believed based on the observation of welded butt joints was that transverse cumulative plastic strain, $\Sigma\varepsilon_{yy}^{p}$, would cause bend-up angular distortion. However, as shown in Fig. 16A, PDA shows that transverse cumulative plastic strain results in bend-down angular dis-

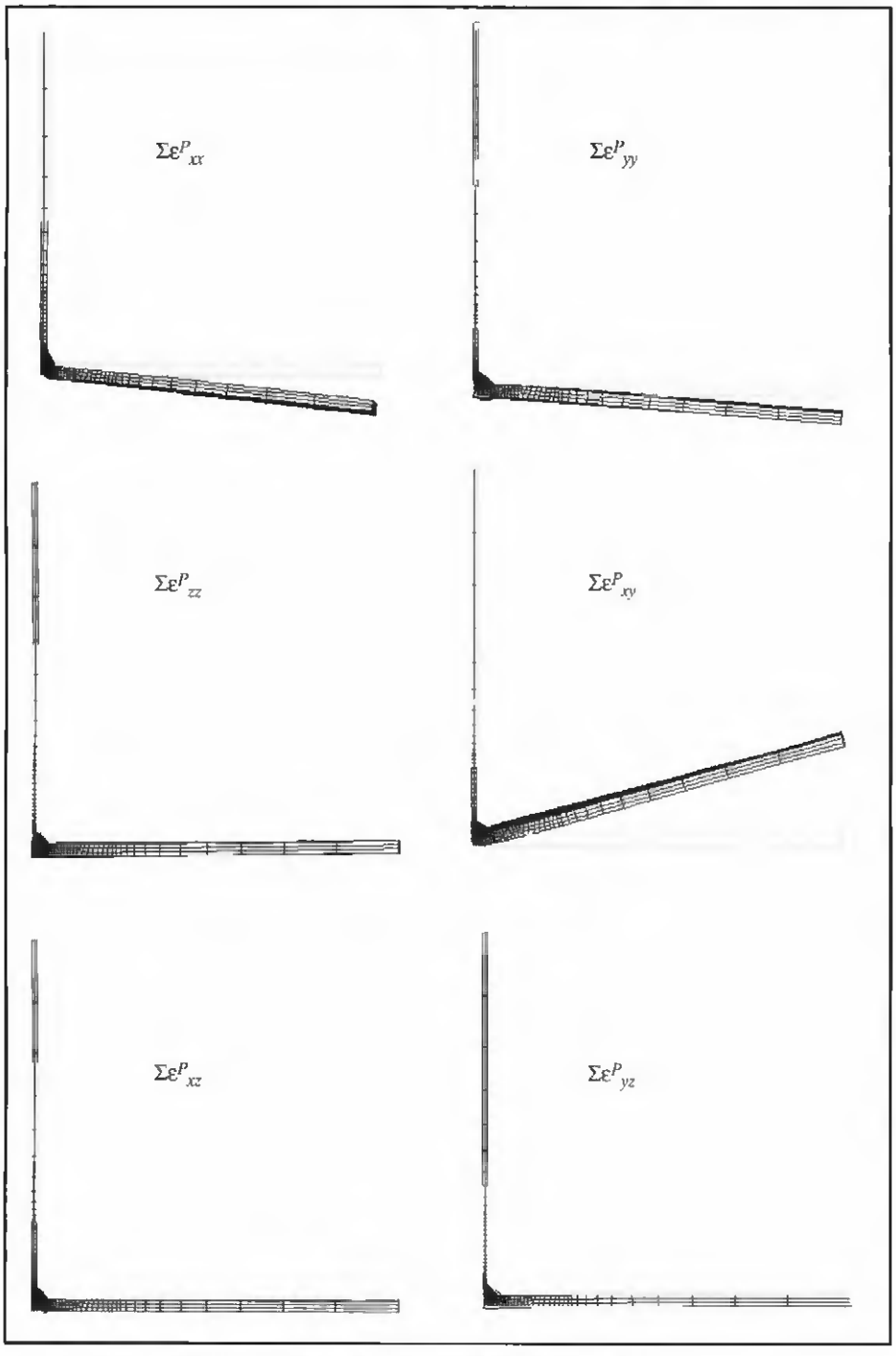

Fig. 16 — Deformed shapes associated with each cumulative plastic strain.

tortion. Vertical cumulative plastic strain, $\Sigma\varepsilon^P_{yy}$, also generates bend-down angular distortion. A slight bend-up angular distortion is produced by longitudinal cumulative plastic strain, $\Sigma\varepsilon^P_{xx}$, which may be mainly related to longitudinal bending and buckling.

All three of the above-mentioned components are nominal components that have been taken into consideration in the distortion analysis. However, the other three shear cumulative plastic strain components have never been highlighted in the distortion analysis. As shown in Fig. 16D, *xy*-plane shear cumulative plastic strain, $\Sigma\varepsilon^P_{xy}$, produces the most bend-up angular distortion. Figure 16E and F shows that the other shear cumulative plastic strains are not related to angular distortion.

In order to clearly show the contribution of each cumulative plastic strain to the total angular distortion, the averaged individual and total angular distortions from PDA and the angular distortion from the elastic-plastic analysis along the free edge line of the flange plate (X=100 mm, Y=3.2 mm in Fig. 4), were plotted using a bar chart, as shown in Fig. 17. It shows clearly the relationship between cumulative plastic strains and angular distortion quantitatively:

- Transverse and vertical cumulative plastic strains result in bend-down angular distortion.
- Longitudinal and *xy*-plane shear cumulative plastic strains generate bend-up angular distortion.
- Most bend-up angular distortion is induced by *xy*-plane shear cumulative plastic strain.
- Angular distortion induced by other shear cumulative plastic strains is small enough to be negligible.

Therefore, without considering the effect of *xy*-plane shear and vertical cumulative plastic strains, the inherent strain model incorporating only transverse cumulative plastic strain may not predict the correct angular distortion pattern in fillet welded T-joints.

The accuracy of the PDA was evaluated. The averaged total angular distortion at the free edge of the flange plate (X=100 mm, Y=3.2 mm in Fig. 4) is 1.01 mm and 1.04 mm in the PDA and the EPA, respectively, as shown in Fig. 17. Using Equation 4, the error is only 3.0%, which is acceptable.

The unique relationship between cumulative plastic strains and angular distortion on this T-joint was investigated by comparing the averaged three displacements at the free edge of the flange plate. Table 4 shows that the linear superposition and the unique relationship between cumulative plastic strains and distortions are valid even though the mapping error exists. This implies that the application of elastic models with material properties at room temperature and cumulative plastic strains (or equivalent forces and moments) is valid in engineering applications.

Conclusions

From the PDA for fillet welded, thin-plate T-joints, the following results were obtained.

- The relationship between cumulative plastic strains and angular distortion is unique.
- Plasticity-based distortion analysis (PDA) was proved to be an effective tool to investigate the relationship between cumulative plastic strains and angular distortion.
- New knowledge about the angular distortion mechanism for fillet welded T-joints obtained from the PDA was addressed:

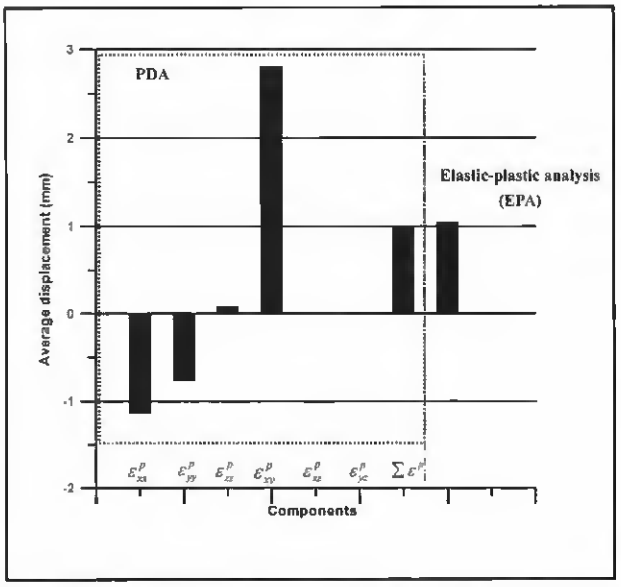

Fig. 17 — Averaged angular distortions calculated by EPA and PDA.

1) *xy*-plane shear cumulative plastic strain produces most bend-up angular distortion, and other shear components are not related with angular distortion.

2) Transverse and vertical cumulative plastic strains result in bend-down angular distortion.

3) Longitudinal cumulative plastic strain produces a slight bend-up angular distortion.

• It was demonstrated that the application of an elastic model using material properties at room temperature and cumulative plastic strains (or equivalent forces and moments) is valid in the distortion analysis.

• In the case of using the inherent strain model in prediction of angular distortion in T-joints, the right angular distortion pattern cannot be obtained by transforming only transverse cumulative plastic strain into equivalent forces and moments. The effect of transverse, vertical, longitudinal, and *xy*-plane shear cumulative plastic strains should be employed in calculation of equivalent forces and moments.

References

1. Ueda, Y., Fukuda, K., and Tanigawa, M. 1979. New measuring method of three dimensional residual stresses based on theory of inherent strain. *Trans. of JWRI* 8(2): 249–256.

2. Ueda, Y., and Yuan, M. G. 1993. Prediction of residual stresses in butt welded plates using inherent strains. *Trans. of the ASME, Journal of Engineering Materials and Technology* 115(10): 417–423.

3. Ma, N. X., Ueda, Y., Murakawa, H., and Maeda, H. 1995. FEM analysis of 3-D welding residual stresses and angular distortion in T-type fillet welds. *Trans. of JWRI* 24(2): 115–122.

4. Yuan, M. G., and Ueda, Y. 1996. Prediction of residual stresses in welded T- and I-joints using inherent strains. *Journal of Engineering Materials and Technology* 118(4): 229–234.

5. Jang, C. D., Seo, S. I., and Ko, D. E. 1995. A study on the simulation of line heating process using a simplified thermal elasto-plastic analysis method. *Journal of Ship Production* 13(1).

6. Luo, Y., Murakawa, H., and Ueda, Y. 1997. Prediction of welding deformation and residual stress by elastic FEM based on inherent strain (Report I) – Mechanism of inherent strain production. *Trans. of JWRI* 26(2): 49–57.

7. Son, K. J., Yang, Y. S., and Beom, H. G. 2000. Analysis of angular distortion in weldments using laminated plate theory. *Science and Technology of Welding and Joining* 5(4): 245–249.

8. Han, M. S. 2002. Fundamental studies on welding-induced distortion in thin plate. Ph.D. dissertation. The Ohio State University, Columbus, Ohio.

9. Kirillov, V. A. 1960. Angular distortions when welding massive members. *BWRA–Welding Production.*

10. Ohata, M., Toda, Y., Toyoda, M., and Takeno, S. 1999. Control of welding distortion in fillet welds of aluminum alloy thin plates. *Welding International* 13(12): 967–976.

11. *ABAQUS User's Manual.* 1998. HKS Co.

12. Jung, G. H. 2003. Plasticity-based distortion analysis for fillet welded thin plate T-joints. Ph.D. dissertation. The Ohio State University, Columbus, Ohio.

13. *ASM Handbook Vol. 6: Welding, Brazing, and Soldering.* 2000. ASM International, Materials Park, Ohio.

14. International Magnesium Association. *Mg Database. http://www. intlmag.org.*

15. Goldak, J., Charkravarti, A., and Bibby, M. 1984. New finite element model for welding heat sources. *Metallurgical Trans. B* 15B: 300–305.

16. Nguyen, N. T., Ohta, A., Matsuoka, K., Suzuki, N., and Maeda, Y. 1999. Analytical solutions for transient temperature of semi-infinite body subjected to 3-D moving heat sources. *Welding Journal* 78(8): 265-s to 274-s.

17. *Metals Handbook 9th Ed. Vol. 2: Properties and Selection: Nonferrous Alloys and Pure Metals.* 1979. ASM. 553–595.

18. Chaboche, J. L. 1986. Time independent constitutive theories for cyclic plasticity. *International Journal of Plasticity* 2(2): 247–302.

19. Kim, Y. C., Chang, K. H., and Horikawa, K. 1998. Production mechanism of out-of-plane deformation in fillet welding. *Trans. of JWRI* 27(2): 107–113.

IIW Annual Assembly Convenes in Japan

The 57th Annual Assembly of the International Institute of Welding (IIW) will be hosted by the Japan Institute of Welding (JIW), at the Osaka International Convention Center, Osaka, Japan, July 11–16, 2004

The IIW is the global body in the science and application of joining technology providing networking and knowledge exchange. Its technical field encompasses the joining, cutting, and surface treatment of metallic and nonmetallic materials by such processes as welding, brazing, soldering, thermal cutting, thermal spraying, adhesive bonding, and microjoining and embraces allied fields including quality assurance, nondestructive testing, standardization, inspection, health and safety, education, training, qualification, design, and fabrication.

The United States will be represented by members of The American Council of the IIW, which is the United States' national committee for the IIW. As a comprehensive forum for professional cooperation through interaction with representatives of the other 41 member countries, the IIW provides a unique opportunity for sharing technological innovations and can be an important avenue for international trade.

For further information on the IIW and membership on The American Council, please contact Andrew Davis, Managing Director, Technical Services Division, at *adavis@aws.org*, (305) 443-9353, ext. 466; or Gricelda Manalich, IIW Coordinator, at *gricelda@aws.org*, (305) 443-9353, ext. 294. Further information, including registration forms, can also be obtained from the IIW Secretariat in Paris, France, at *www.iiw-iis.org*.